A Volcano Rekindled: The Renewed Eruption of Mount St. Helens, 2004–2006
Edited by David R. Sherrod, William E. Scott, and Peter H. Stauffer
U.S. Geological Survey Professional Paper 1750, 2008

Chapter 13

Effects of Lava-Dome Growth on the Crater Glacier of Mount St. Helens, Washington

By Joseph S. Walder[1], Steve P. Schilling[1], James W. Vallance[1], and Richard G. LaHusen[1]

Abstract

The process of lava-dome emplacement through a glacier was observed for the first time as the 2004–6 eruption of Mount St. Helens proceeded. The glacier that had grown in the crater since the cataclysmic 1980 eruption was split in two by the new lava dome. The two parts of the glacier were successively squeezed against the crater wall. Photography, photogrammetry, and geodetic measurements document glacier deformation of an extreme variety, with strain rates of extraordinary magnitude as compared to normal temperate alpine glaciers. Unlike such glaciers, the Mount St. Helens crater glacier shows no evidence of either speed-up at the beginning of the ablation season or diurnal speed fluctuations during the ablation season. Thus there is evidently no slip of the glacier over its bed. The most reasonable explanation for this anomaly is that meltwater penetrating the glacier is captured by a thick layer of coarse rubble at the bed and then enters the volcano's groundwater system rather than flowing through a drainage network along the bed. Mechanical consideration of the glacier-squeeze process also leads to an estimate for the driving pressure applied by the growing lava dome.

Introduction

Since October 2004, a silicic lava dome has been emplaced first through, and then alongside, glacier ice in the crater of Mount St. Helens. The dome has been emplaced in a near-solid state, not as liquid magma solidifying at the Earth's surface (Vallance and others, this volume, chap. 9). Heretofore, dome emplacement through a glacier was known only from a single published photograph (Simons and Mathewson, 1955, plate 6) showing a lava dome that had been emplaced through the caldera glacier of Great Sitkin Volcano, Alaska, sometime in 1945. Evidence bearing on lava-dome emplacement into ice has been presented by, for example, Gilbert and others (1996), who used geophysical methods to identify lava domes emplaced beneath the caldera glacier of Volcán Sollipulli, Chile, and by Tuffen and others (2001), who described a domelike rhyolite body that was evidently emplaced subglacially in Iceland and since exhumed. The 2004–6 eruption of Mount St. Helens has afforded the first-ever opportunity to actually document the process of lava-dome emplacement through a glacier.

The common picture of volcano-glacier interactions is one of rapid meltwater generation either as magma contacts the glacier bed—examples from Iceland have been especially well characterized, for example, the 1996 Gjálp eruption (Guðmundsson and others, 1997)—or as lava or pyroclasts are erupted onto the glacier surface (many examples are mentioned by Major and Newhall, 1989). At Mount St. Helens, however, glacier melt associated with dome emplacement has been minor, even as the glaciological consequences have been dramatic—Crater Glacier has been cut in half, and the resulting ice bodies have in succession been squeezed between the growing lava dome and the crater wall. In this paper we focus our attention on the glaciological consequences of the eruption. Condensed discussions of this material have been presented elsewhere by Walder and others (2005, 2007).

Field Setting: Crater Glacier Before October 2004

After the cataclysmic eruption of May 18, 1980, which beheaded, and in some cases completely destroyed, the glaciers that existed on the flanks of Mount St. Helens (Brugman and Meier, 1981), material from rock and snow avalanches began accumulating in the north-facing, amphitheaterlike crater (fig. 1). Mills (1992) used digitized topographic maps to

[1] U.S. Geological Survey, 1300 SE Cardinal Court, Vancouver, WA 98683

calculate the volumes of material eroded from the crater walls and accumulated on the crater floor. His results show that as of mid-1988, the thickness of accumulated material was 60 to 80 m across much of the crater floor south of the 1980–86 lava dome. The accumulated material as of mid-1988 was about 60 percent rock debris by volume and contained interstitial snow, but it was not flowing. The first reasonably clear evidence that a crater glacier had come into existence—the appearance of crevasses, which reflect flow—comes from photographs taken in September 1996 (Schilling and others, 2004). The glacier (now called Crater Glacier) at that time had a surface area of about 0.1 km^2; by September 2000, this area had increased to about 1 km^2. Proceeding similarly to Mills (1992) but using digital elevation models (DEMs), Schilling and others (2004) calculated that the material that had accumulated in the crater between May 18, 1980, and September 2000 had a thickness locally as great as 200 m and a volume of 1.2×10^8 m^3, of which about one-third comprised rock debris. If we interpret these figures in the context of Mills' discussion of what had accumulated on the crater floor as of 1988, it seems clear that the deepest part of the crater-floor fill consists primarily of rock-avalanche debris—a point to which we shall return—and would not be considered glacier ice by usual glaciological standards. The uppermost part of Crater Glacier, however, probably contains no more than 5 percent rock debris by volume, with such debris forming discrete, discontinuous layers that originate as rock-avalanche lobes (fig. 2), and glaciologists would call this material "dirty" firn and glacier ice.

To what extent is the material accumulated on the crater floor since 1980 a glacier? In framing an answer, we have to make explicit our reason for asking the question in the first place. Our focus here is not on morphology, but rather on the ice flow and deformation processes familiar to glaciologists, and how such processes affect the mechanical response of the crater-fill material to lava-dome emplacement. From this perspective, what one is tempted to call a glacier in a morphological sense is not the same as what is rheologically and mechanically glacier ice. Deformation of a material containing 60 percent rock debris by volume—Mills' (1992) estimate for the composition of the pre-1988 crater-floor fill—is surely dominated by rock-to-rock friction, not creep of any interstitial ice.

We choose to exclude from our mechanically defined glacier, as best we can, the deepest, rock-rich crater-floor fill. We do this by picking the glacier bed as the crater-floor surface

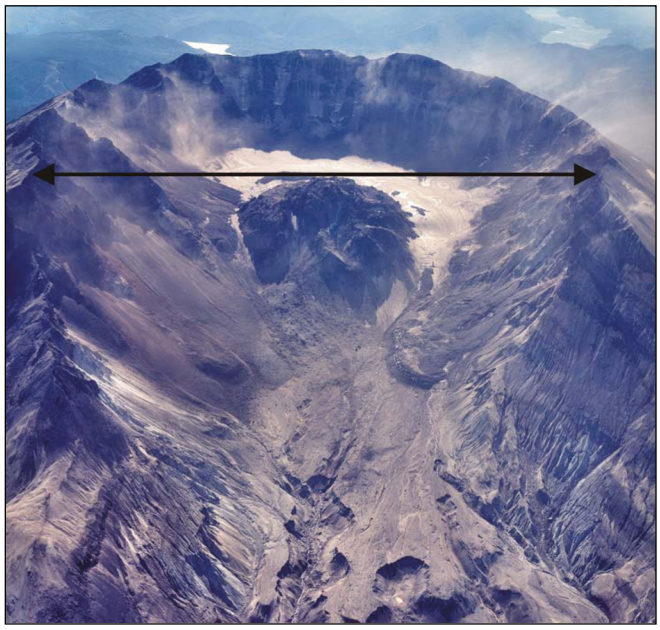

Figure 1. Oblique view of Mount St. Helens crater on October 5, 2000, looking south. Crater Glacier wraps around 1980–86 lava dome. East (left) arm of glacier is obscured by rock-avalanche debris; west (right) arm merges to the north of the lava dome with a rock-covered icy mass shed off the west crater wall. Crater width, as indicated by double-headed arrow, is about 2 km. USGS photograph by Bergman Photographic Services, Portland, Oreg.

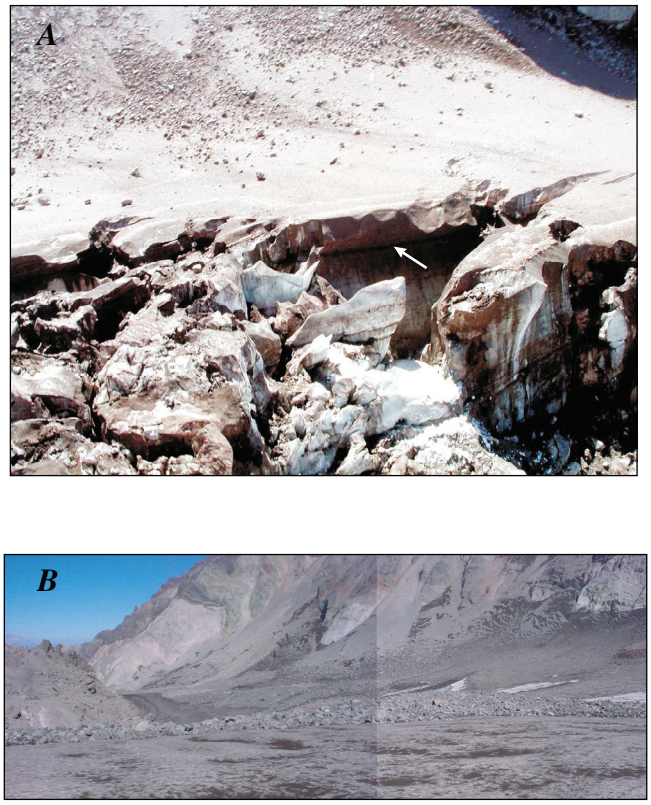

Figure 2. Glacier features in crater of Mount St. Helens. *A*, Rock layers within uppermost part of Crater Glacier, as exposed on west side of new lava dome. Distance from glacier surface to prominent debris layer (arrow) is about 3 to 5 m. View to east. USGS photograph taken August 4, 2005, by W.P. Johnson. *B*, Surface of Crater Glacier on August 20, 2003, looking north along east side of 1980–86 lava dome. Rock-avalanche lobe in center of view extended from the crater wall nearly to the south side of the lava dome and had maximum thickness of about 1 m. USGS photograph by J.S. Walder.

defined by DEMs for October 12, 1986, and November 12, 1986. This is an approximate but defensible choice for several reasons: (1) The rate of accumulation of rock debris in the crater decreased markedly after 1986 (fig. 3). (2) 1986 marks the end of the previous dome-growth episode, so accumulation after 1986 occurred within a basin with reasonably stable boundaries. (3) As we argue in appendix 1, interstitial ice within the lowest, rock-rich crater-fill material has probably melted and not been replaced by ice intruding from above. With the 1986 surface thus defined as the glacier bed, we then differenced 2003 and 1986 DEMs to calculate the glacier thickness shortly before the start of the 2004 eruption (fig. 4). Using the Mills (1992) and Schilling and others (2004) figures for rock-debris accumulation, we estimate that Crater Glacier, so defined, has an average rock content of 15 percent by volume.

A note about names. The U.S. Board on Geographic Names on June 6, 2006, approved the name "Crater Glacier" for the feature that existed before the recent eruption. However, as is documented below, Crater Glacier has been split in two by dome growth, and it is both sensible and convenient to use the informal names "west Crater Glacier" and "east Crater Glacier" for the ice masses that exist in the crater as of the time of writing.

Changes in Crater Glacier Since October 2004

Methods

Hazards posed by Mount St. Helens' eruptions severely restricted field work in the crater, so we documented eruptive effects on Crater Glacier primarily by photography and photogrammetry. We managed to collect some glacier-motion data using single-frequency global positioning system (GPS) stations slung by helicopter onto the glacier surface in 2005 and 2006. The GPS stations (LaHusen and others, this volume, chap. 16) were available for glacier monitoring only intermittently, and on several occasions had to be moved, or else they would have toppled into crevasses. Station positions were determined from short-baseline differential fixed static solutions sampled at 10-second intervals over a 25-minute period every hour. Accuracy of individual solutions was approximately 20 mm in the horizontal and 50 mm in the vertical. A running-median filter was applied to solutions to remove spikes.

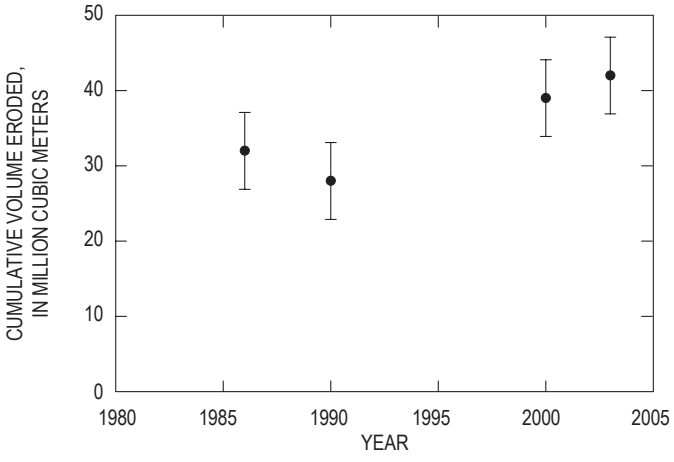

Figure 3. Cumulative volume eroded from walls of Mount St. Helens crater since the 1980 eruption, as determined by differencing digital elevation models for 1990, 2000, and 2003 with a DEM for 1980. Error bars (±1σ) are shown. Despite uncertainties in the data, it is clear that erosion rate has fallen sharply since the mid-1980s.

Morphological Changes

One of the first indirect signs of dome growth was the formation of a bulge in the south part of Crater Glacier during the last few days of September 2004 (fig. 5). An explosion on October 1, 2004, excavated a hole in the glacier (fig. 6). As the eruption proceeded, the southern part of Crater Glacier was eventually punctured by a rock spine surrounded by rubble (fig. 7), the latter perhaps comprising unconsolidated mate-

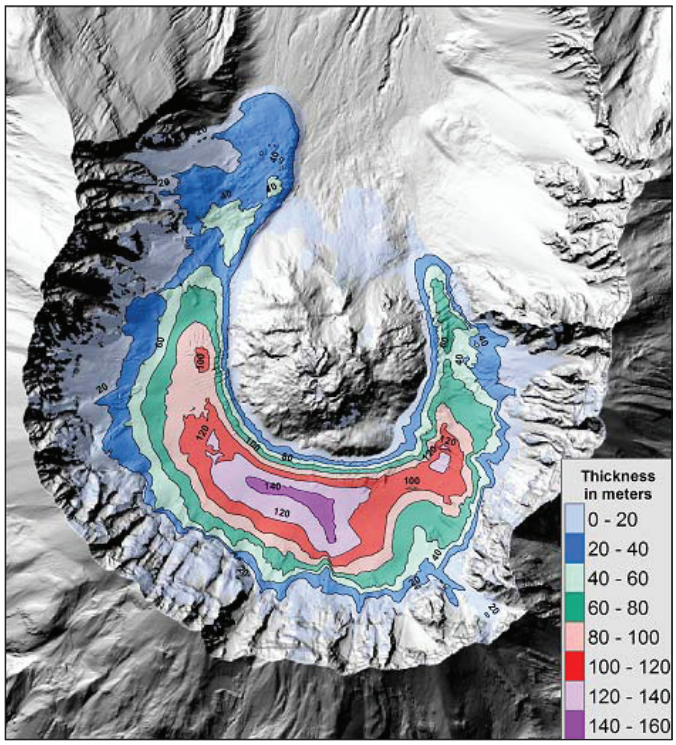

Figure 4. Map showing thickness of material accumulated on the crater floor of Mount St. Helens between October–November 1986 and September 2003. Background is a hillshade-relief map constructed from September 2003 digital elevation model. The 1980–86 lava dome is in center. As explained in text, the October–November 1986 surface is approximately the glacier bed, and the isopachs represent approximate glacier thickness.

rial that underlay the glacier. The lava dome as it exists as of October 4, 2006, is a complex of seven such spines extruded sequentially in the solid state from the same general vent area (fig. 8; Vallance and others, this volume, chap. 9). Spine 3, which began to be extruded in late October 2004, grew preferentially southward, developing a whaleback form and pushing aside firn and ice in a way reminiscent of the bow wave that precedes a ship through water (fig. 9). After spine 3 ran into the south crater wall in mid-November 2004, Crater Glacier was for all practical purposes split into two parts.

East Crater Glacier

Spine 3 spread to the east until late December 2004, then spalled greatly and was shouldered aside by spine 4—another "whaleback"—which grew until mid-April 2005. The east Crater Glacier (ECG) was effectively caught in a vise formed by the whaleback spines and the east crater wall. Owing to drought conditions that prevailed throughout most of the winter of 2004–5, there was practically no snow accumulation, and thus glacier-surface features showed very clearly. As eastward dome growth proceeded, the upwarped glacier apron on the east side of the dome (compare fig. 9) impinged against the east crater wall. However, the northernmost part of this ice apron was rotated until it formed a steplike feature trending nearly east to west (fig. 10). The ECG surface buckled, with east-west-trending crevasses forming parallel to the direction of dome spreading (fig. 11). Comparison of DEMs reveals that between mid-November 2004 and mid-April 2005, the dome/ECG contact migrated laterally by as much as 200 to 250 m and the glacier locally doubled in thickness (figs. 12, 13, 14). Expressed in terms of rates, the dome-ECG contact moved on average about 1 m/d and the glacier thickened at an astounding 0.6 m/d. By way of comparison, the average thickening rate for the "reservoir area" of a surging glacier, during the interval between surges, is perhaps 0.02 to 0.04 m/d (Raymond, 1987, p. 9123, fig. 1).

Since spine 4 quit growing in mid-April 2005, east Crater Glacier has thinned in its upper reach and thickened in its lower reach as normal flow processes redistribute ice mass downslope. Longitudinal crevasses became obvious by late April 2005; these crevasses probably reflect transverse spreading as the bowed-up surface—so evident during the squeezing episode—relaxed. As a result, the glacier surface became a field of seracs (fig. 15). The ECG terminus became steep (fig. 16) and advanced by about 150 m between April 19, 2005, and August 18, 2006.

Figure 5. Bulge in Crater Glacier next to south side of 1980–86 lava dome on September 30, 2004. Dark material on surface of fractured area is talus. Width of bulge is about 50 m. View to west. USGS photograph by D. Dzurisin.

Figure 6. Beginning of Mount St. Helens eruption through Crater Glacier on October 1, 2004. View to west. USGS photograph by J.S. Pallister.

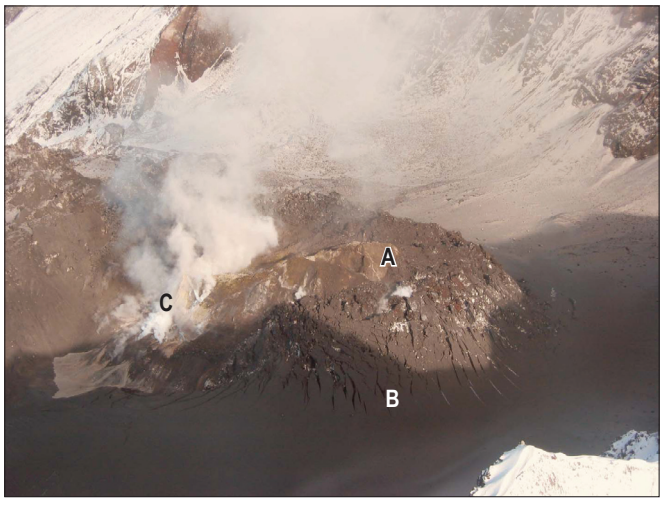

Figure 7. Upwarped, tephra-covered firn and ice around margins of new lava dome on October 11, 2004. View to northeast. A, Deformed rock at ambient temperature. B, Deformed firn and ice. C, Spine 1 (hot rock). USGS photograph by C.A. Neal.

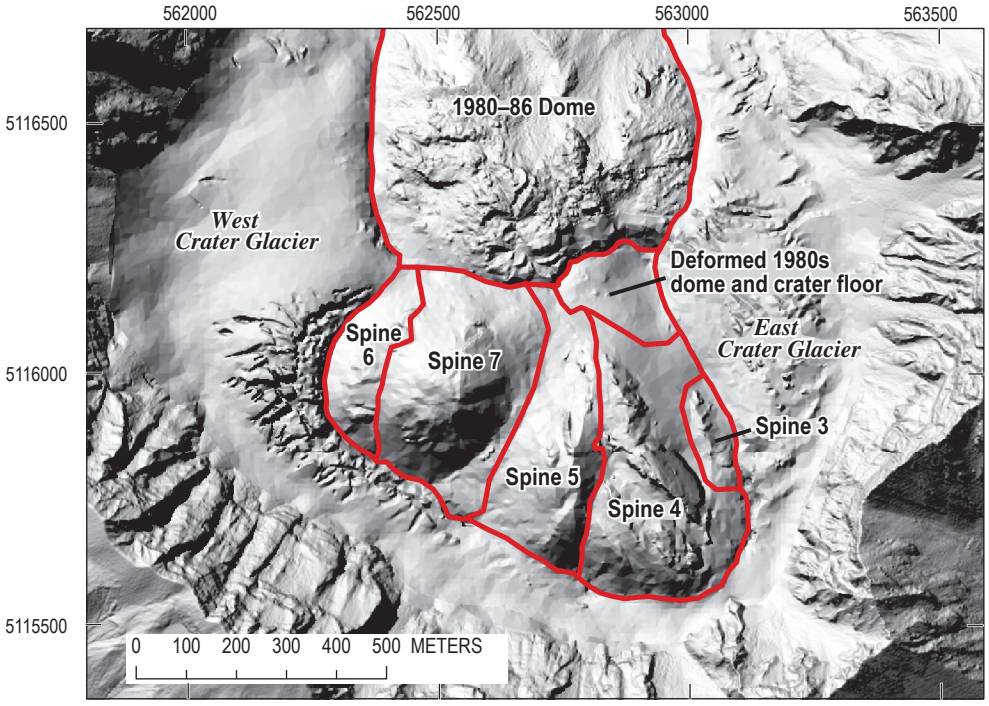

Figure 8. Map of the lava-dome spine complex in Mount St. Helens crater drawn on a hillshade-relief map from the October 24, 2005, DEM. Spines are numbered according to sequence of extrusion events, as discussed by Vallance and others (this volume, chap. 9). Coordinates referable to UTM zone 10, North American datum 1983.

Figure 9. Upwarped firn and ice around margin of new whaleback lava spine, November 20, 2004. View to east. USGS photograph by S.P. Schilling.

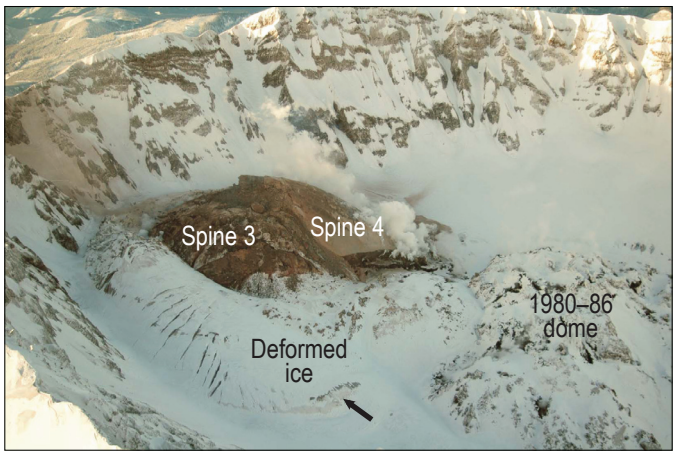

Figure 10. The new lava dome of Mount St. Helens (dominated by spines 3 and 4) and the by-then morphologically distinct east Crater Glacier (in foreground) on January 14, 2005. The bulge indicated by the arrow is not a kinematic wave but was instead formed when upwarped ice around the spine margins (see figs. 7, 8) was rotated as dome growth proceeded to east. View to southwest. USGS photograph by J.W. Vallance.

Figure 11. Upwarped surface of east Crater Glacier on February 16, 2005. View to north. Crevasses are oriented roughly east-west, paralleling direction of squeeze by new lava dome (at left). 1980s dome in left-center distance. USGS photograph by J.S. Walder.

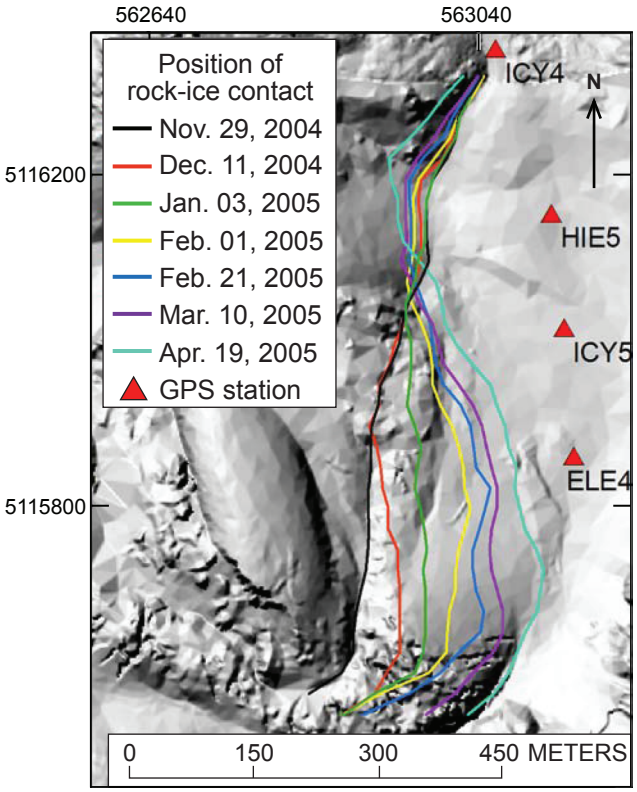

Figure 12. Migration of the contact between rock of the new lava dome and ice of east Crater Glacier during the period from November 29, 2004, to April 19, 2005. Contact position was determined from DEMs, with a probable error of about 5 m. Background image is hillshade-relief map for November 29, 2004. Coordinates are UTM zone 10 easting and northing, North American datum 1983. Eastward migration of rock-glacier contact for northing between about 5115500 and 5116000 reflects growth of new lava dome, which caused the glacier to thicken locally. The resulting enhanced ice flow to the north caused ice to encroach upon the margin of the old (1980–86) lava dome north of about northing 5116050. Also indicated are positions of four GPS stations deployed on the glacier at various times.

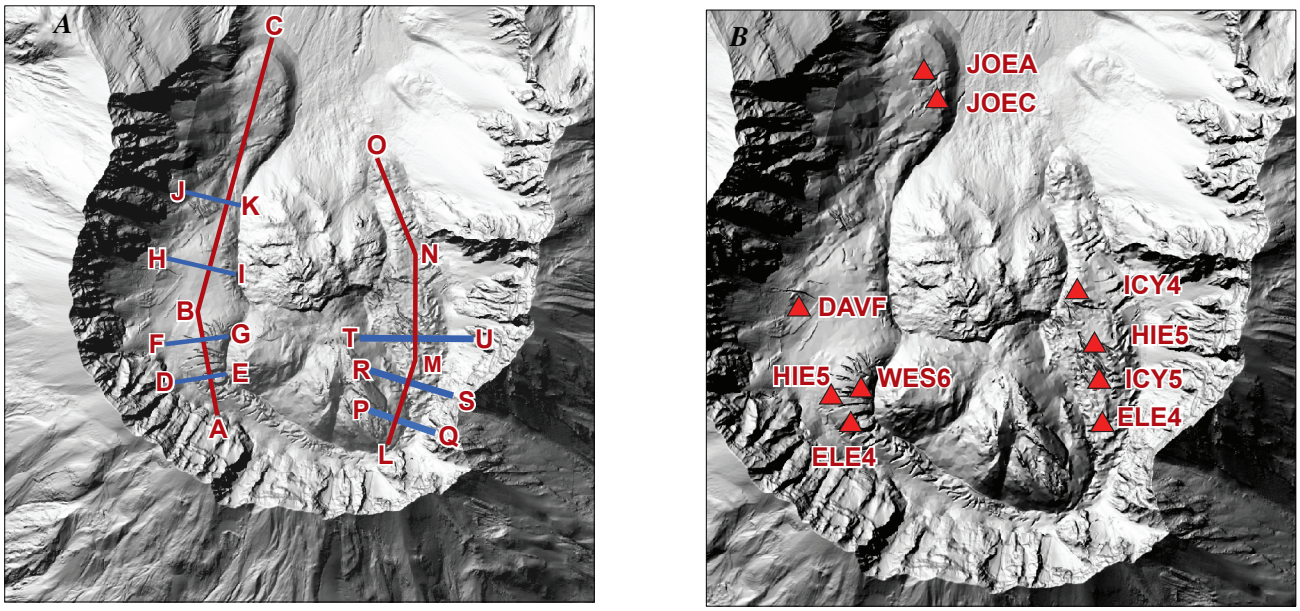

Figure 13. Hillshade-relief maps of Mount St. Helens crater constructed from photogrammetric analysis of aerial photographs dated October 24, 2005. *A*, Lines of section for which we calculated changes in glacier-surface altitude. *B*, Positions of GPS stations. Note that any individual station may not have been on the glacier on the date of the photographs. ELE4 appears twice because it was shifted from east Crater Glacier to west Crater Glacier during the course of the eruption.

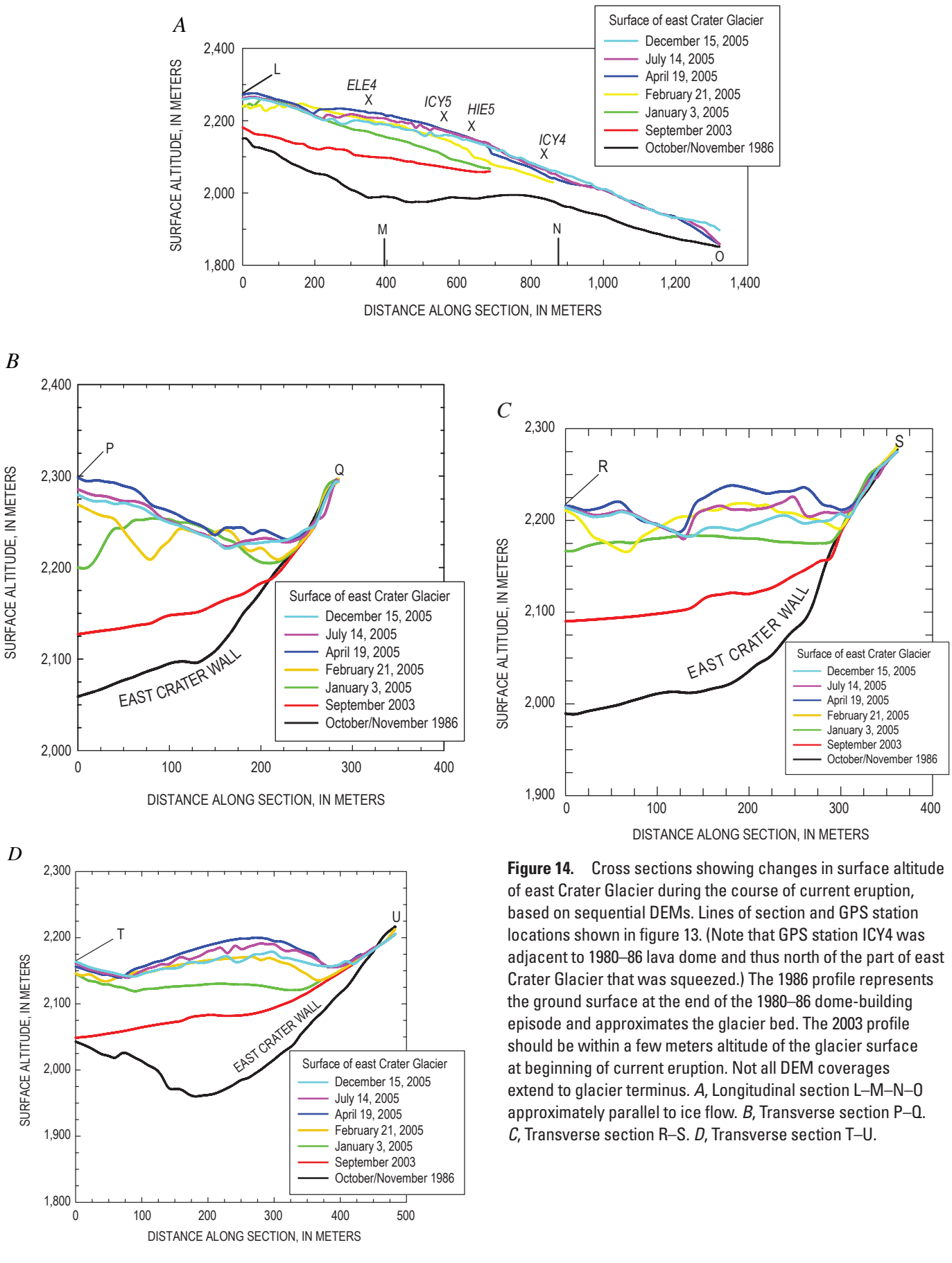

Figure 14. Cross sections showing changes in surface altitude of east Crater Glacier during the course of current eruption, based on sequential DEMs. Lines of section and GPS station locations shown in figure 13. (Note that GPS station ICY4 was adjacent to 1980–86 lava dome and thus north of the part of east Crater Glacier that was squeezed.) The 1986 profile represents the ground surface at the end of the 1980–86 dome-building episode and approximates the glacier bed. The 2003 profile should be within a few meters altitude of the glacier surface at beginning of current eruption. Not all DEM coverages extend to glacier terminus. *A*, Longitudinal section L–M–N–O approximately parallel to ice flow. *B*, Transverse section P–Q. *C*, Transverse section R–S. *D*, Transverse section T–U.

West Crater Glacier

Growth of spine 6 (Vallance and others, this volume, chap. 9) adjacent to west Crater Glacier (WCG) became noticeable in early August 2005. Surface bulging and crevassing of the glacier proceeded in much the same way as with ECG (fig. 17). Spine 6 quit growing, and spine 7 began growing and overriding spine 6, in early to mid-October 2005, but WCG continued to be squeezed owing to the push exerted by spine 7 on spine 6. Events unfolded much as with ECG: The dome-WCG contact migrated locally by >200 m (fig. 18), and the glacier locally doubled in thickness (fig. 19). A distinct bulge in the WCG surface began propagating downglacier (fig. 19*A*) and impinged upon the rather flat, mostly rock-covered terminus region, which arguably originated as a separate mass shed from the west crater wall (compare fig. 1). In summer 2006, it became clear that advance of the bulge was being accommodated by development of a shear zone within the flat terminus region (fig. 20).

Figure 15. Crevasses formed by lava-dome growth at Mount St. Helens. *A*, Longitudinal crevasses on east Crater Glacier cutting across transverse crevasses that had formed during eastward lava-dome growth (compare fig. 9), as seen on May 12, 2005. View to southwest. USGS photograph by M. Logan. *B*, Part of east Crater Glacier on July 26, 2005. View to south. Longitudinal crevasse growth by this date had effectively chopped the glacier surface into a field of seracs. USGS photograph by S.P. Schilling.

Change in Ice Volume During the Eruption

The change in glacier volume during the course of the eruption can be determined by comparing DEMs prepared for different dates. The method is discussed in appendix 2, and results are summarized in figure 21. The estimated volume decrease from the start of the eruption (October 2004) until October 2005—meaning (approximately) from the end of one ablation season to the end of the next ablation season—was $6.7\pm3.7\times10^6$ m^3, corresponding to an average rate of loss of 0.21 ± 0.12 m^3/s. The eruption has clearly not been marked by a process commonly associated with volcano-glacier interactions, namely, rapid meltwater generation (Major and Newhall, 1989). In retrospect, this is unsurprising—the eruption has been predominantly quiescent, not explosive, so scouring of the glacier surface by hot fragmental flows has been negligible; moreover, the spines have been extruded in a solid state, with surface temperature well below the solidus, and the glacier is well insulated from them by rubble (Schneider and others, this volume, chap. 17).

Ice Dynamics

Given the radical morphological changes to Crater Glacier during the eruption, described above, we should not be surprised if the glacier's dynamics were also significantly affected. Unfortunately, our complete lack of data on glacier-surface speed before the 2004 eruption complicates an assessment of how the eruption affected glacier dynamics. To try to infer a rough baseline for preeruption dynamics, we use mass-balance considerations to estimate the so-called balance velocity U_b, which is the cross-sectionally averaged speed that a glacier would have if it were in steady state (Paterson, 1994, p. 250):

$$U_b(x) = \frac{1}{W(x)\bar{H}(x)} \int_0^x \dot{b}(\xi) W(\xi)\, d\xi \quad , \qquad (1)$$

where $W(x)$ is glacier width at distance x from the "headwall" or upstream end (in this case, the south crater wall), $\bar{H}(x)$ is average depth at a cross section, and $\dot{b}(x)$ is the local mass

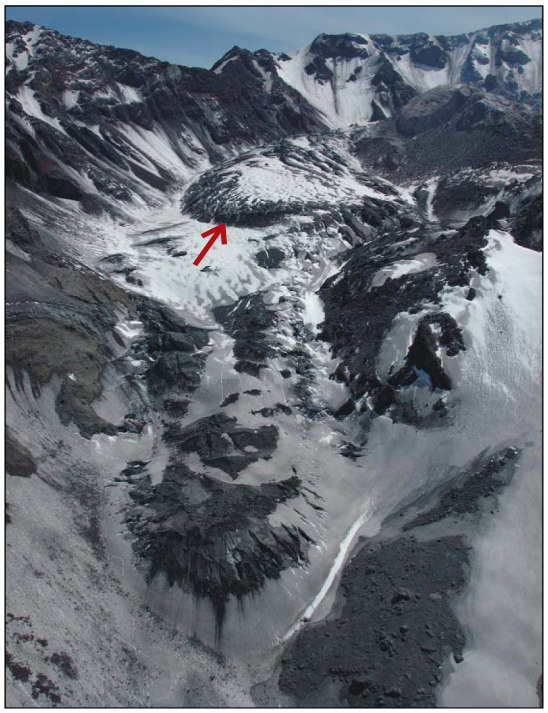

Figure 16. Terminus (lower center) of east Crater Glacier on June 15, 2005. View to south. Compare to indistinct terminus as seen about 5 years earlier (fig. 1). Arrow indicates bulge similarly indicated in figure 10. The glacier is only about 100 to 150 m wide where it passes between crater wall and old lava dome (right center) USGS photograph by S.P. Schilling.

balance expressed as a thickness per unit time. Equation 1 is simply a mathematical statement of the steady-state assumption, namely, that the glacier is neither thickening nor thinning. We apply equation 1 to what would become (during the eruption) east Crater Glacier and estimate U_b near the terminus (at a position we denote by $x = L$) by taking $L \approx 1.2$ km, $\bar{H} \approx 60$ m (fig. 14*A*), and an average value $\dot{b} \approx 4$ m/yr (from a total ice accumulation of about 80×10^6 m^3 over an area of about 1 km^2

Figure 17. West Crater Glacier adjacent to westward-growing lava dome as seen on September 2, 2005. View to southeast. The crevasse pattern in the glacier is complicated and reflects shifting directions of dome growth, but those crevasses normal to the dome-glacier margin are the youngest.
USGS photograph by M. Logan.

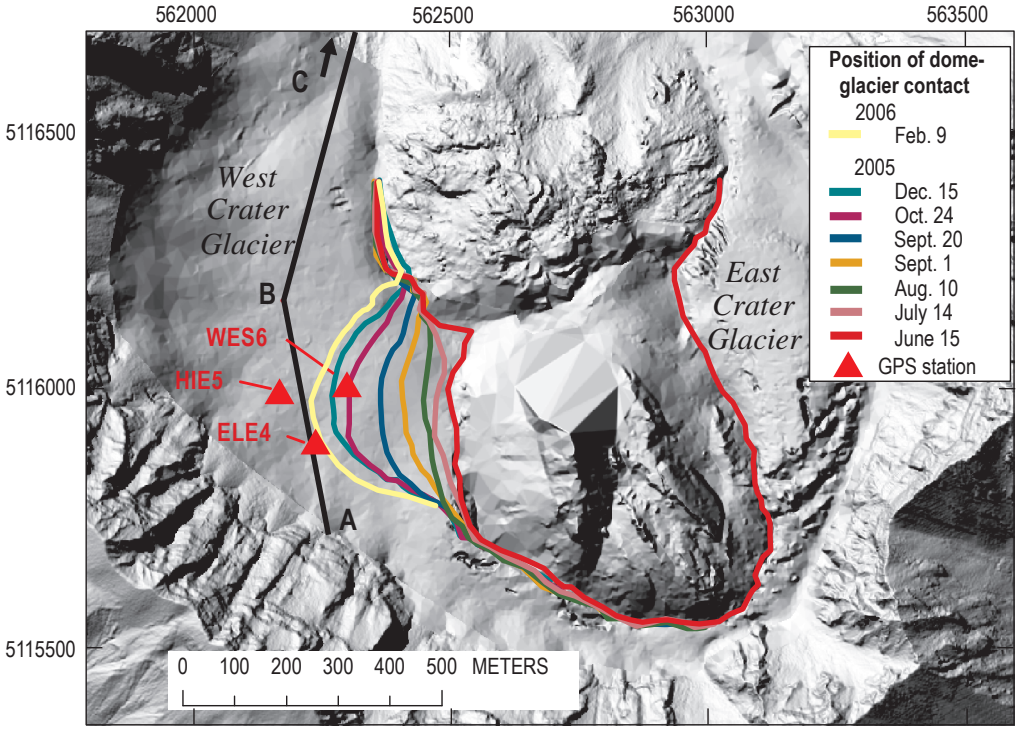

Figure 18. Migration of contact between the new lava dome and west Crater Glacier during the period June 15, 2005, to February 9, 2006. Contact position was determined from DEMs, with a probable error of about 5 m. Background image is hillshade-relief map for June 15, 2005. Coordinates are UTM zone 10 easting and northing, North American datum 1983. As the new dome grew, the glacier encroached upon margin of the old (1980–86) lava dome. Also shown are positions of three GPS stations that were deployed on the glacier at various times in 2005.

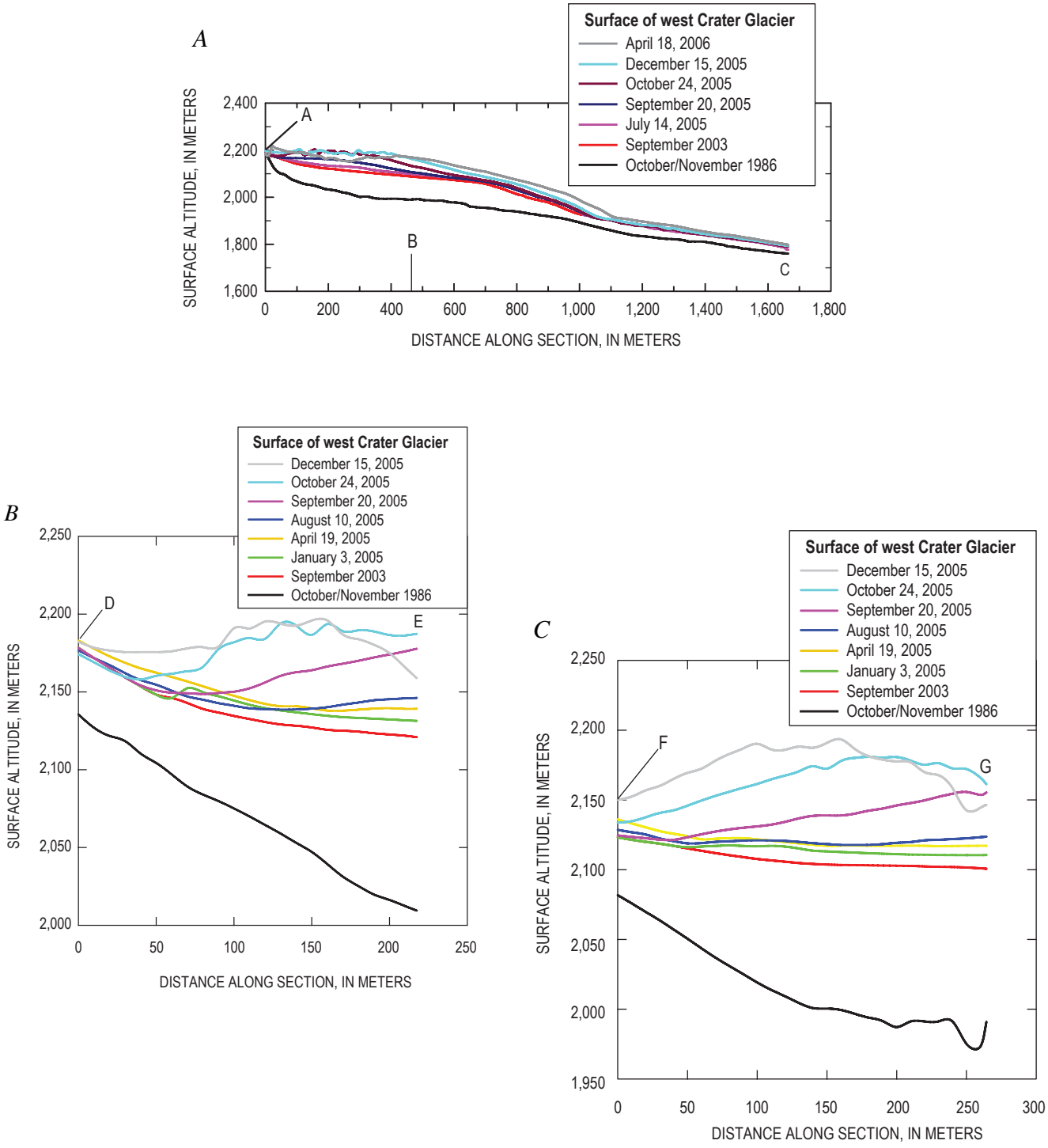

Figure 19. Change in surface altitude of west Crater Glacier during course of ongoing eruption, based on sequential DEMs. Lines of sections shown in figure 13. The 1986 profile represents the ground surface at end of the 1980–86 dome-building episode and is approximately the glacier bed. The 2003 profile should be within a few meters altitude of glacier surface at beginning of current eruption. *A*, Longitudinal section A–B–C, approximately following the thickest ice. The points labeled A, B, and C match those in figure 13*A*. *B*, Transverse section D–E. *C*, Transverse section F–G. *D*, Transverse section H–I. *E*, Transverse section J–K.

in 20 years), and by treating W as a constant. We find $U_b \approx 0.24$ m/d, which corresponds to a surface speed of about 0.29 m/d for ice with the flow-law exponent $n = 3$ (van der Veen, 1999, p. 103–106). We emphasize that this is at best a rough baseline for thinking about the preeruption surface speed, because the glacier was manifestly not in a steady state but rather growing.

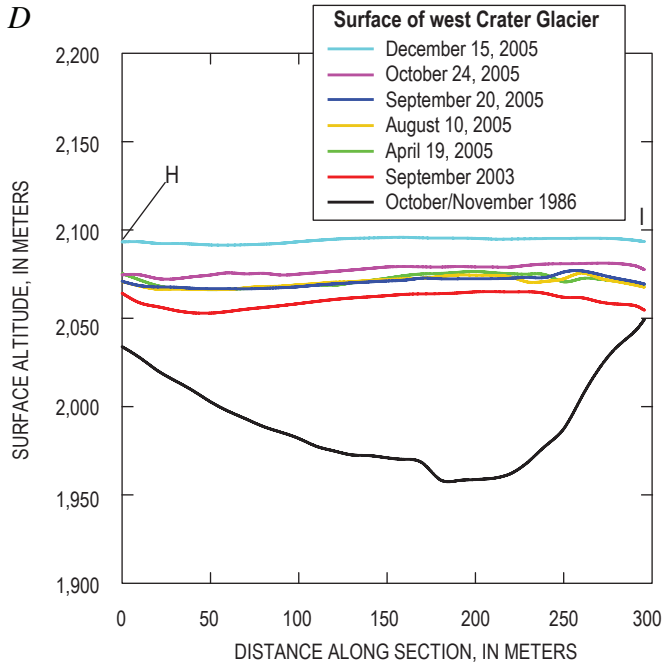

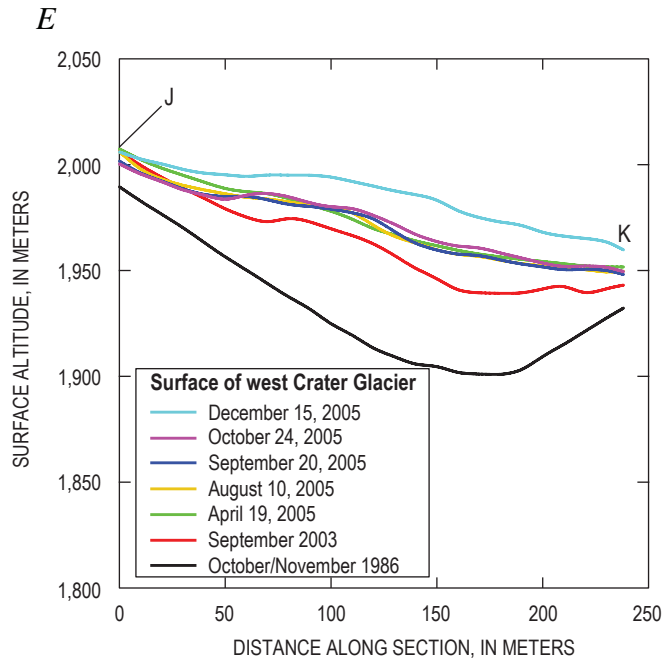

Figure 19—Continued.

East Crater Glacier

The GPS station positions during 2005 are shown in figure 13*B*; measured displacement rates are shown in figure 22. Interestingly, the balance velocity estimated above is comparable to the speed of station ICY4, which was downglacier of the

Figure 20. The glacier in Mount St. Helens crater as seen on September 12, 2006. View to south. As bulge on west Crater Glacier advanced and impinged on relatively flat terminus area, a shear zone delineated by echelon fractures developed (solid red curve). The shear zone at its northern end took on the character of a zone of compression, with crevasses parallel to direction of maximum compression (dotted red lines). Positions of GPS stations JOEA and JOEC are indicated. USGS photograph by W.E. Scott.

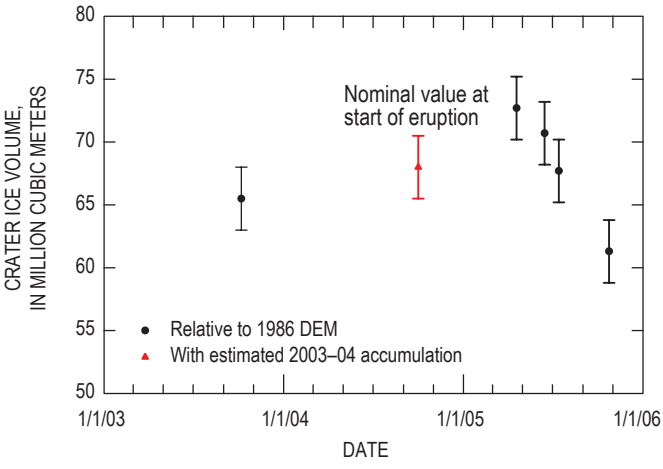

Figure 21. Total volume of glacier in Mount St. Helens crater as a function of time, with error bars (±1σ).

domain squeezed by the lava dome, on ice about 70 m thick and not far from the ECG terminus (fig. 10). In comparison, ICY5, about 300 m upglacier of ICY4, within the glacier reach being squeezed by dome growth (fig. 12) and on ice about 150 m thick, moved about 1.3 m/d, or about four times as fast as ICY4. This comparison presents a conundrum if deformation is only by simple shear and reflects a balance between gravitational driving stress and drag on the glacier bed and sides, in which case the difference in surface velocity between ICY4 and ICY5 should have been a factor of about $(150/70)^{n+1} \approx 21$ for a flow-law exponent $n = 3$ (van der Veen, 1999, p. 103–104). Moreover, owing to the nonlinear rheology of glacier ice (van der Veen, 1999, p. 13–15), the squeeze exerted on east Crater Glacier by the growing lava dome should have reduced the effective viscosity of the ice near ICY5 and made the difference in speed from ICY4 to ICY5 even greater. Resolution of the conundrum involves recognizing that gravitational driving stress is in fact resisted not only by drag but also by gradients in stress along the flow (van der Veen, 1999). A useful mechanical analogy is to think of east Crater Glacier, during the squeezing episode, as a tube of toothpaste with the cap removed. If the entire tube were squeezed uniformly, toothpaste would squirt out rapidly, but if squeezing is applied only to the part of the tube farthest from the opening, the toothpaste nearer the opening acts as a dam. Computational modeling by Price and Walder (2007) has confirmed the existence of a very strong longitudinal stress gradient.

Strain rates associated with ECG deformation can be estimated, in part, by considering the rate of eastward migration of the dome-glacier contact and the rate of glacier-surface uplift. Dividing the rate of eastward migration of the dome-glacier contact near ELE4 (fig. 12) by the glacier width (about 300 m), the average rate of contact migration for the period December 1, 2004, to January 3, 2005, corresponds to a squeeze strain rate of about –0.006/d; for the period January 3, 2005, to April 16, 2005, the squeeze strain rate was about –0.0036/d. Elongational strain rate in the downglacier direction cannot be estimated directly owing to the fact that there were never simultaneously two GPS units on the reach being squeezed. The strain rate associated with glacier thickening for the period January 3, 2005, to April 16, 2005, can be roughly estimated (see fig. 14*A*) at about (0.6 m/d)/(100 m) ≈ 0.006/d near the centerline of east Crater Glacier.

To put the ECG strain-rate values in perspective, consider ice moving through a valley constriction at a rate of 100 m/y, with the valley narrowing by 25 percent over a length of 1 km—arguably a rather severe constriction. The lateral strain rate in this case would be –0.0001/d, or about 1–3 percent of the lateral strain rate associated with squeezing of the ECG. Thickening strain rate as large as that measured at ECG is known only from surge fronts (Kamb and others, 1985; Raymond and others, 1987), although in such cases the maximum compression is oriented along the normal ice-flow direction, whereas with ECG, maximum compression was transverse to the normal ice-flow direction.

West Crater Glacier

The GPS stations on west Crater Glacier during the summers of 2005 and 2006 (fig. 13*B*) recorded the response of the glacier to westward dome growth. We discuss results for 2005 and 2006 separately.

In 2005 (fig. 23), the peak in speed of ELE4 at about day 273 (September 30) occurred a few days before the appearance of spine 7 just east of spine 6 (fig. 8; Vallance and others, this volume, chap. 9). This peak in speed probably reflects a change in the stresses applied to WCG by the dome. During the 23-day period when the GPS records overlapped, all three stations on WCG accelerated rather smoothly (fig. 23*B*); differences in azimuth of motion reflect the local direction of dome growth. The displacement records for the overlap

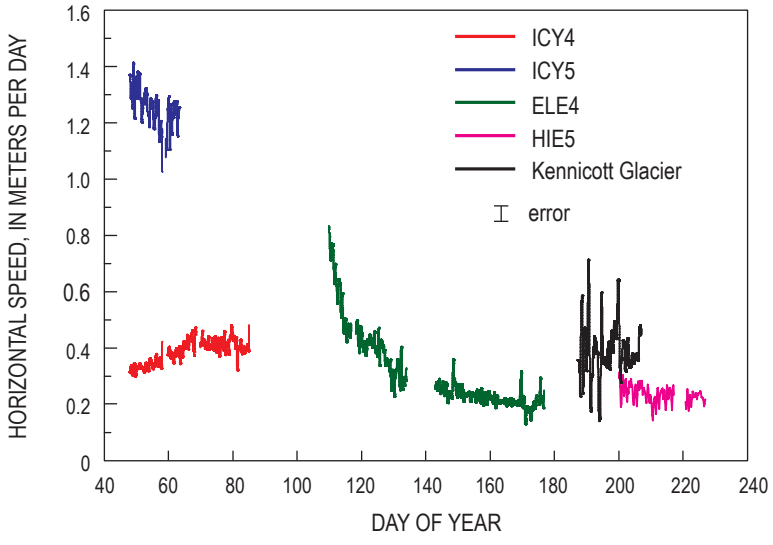

Figure 22 Horizontal speed of east Crater Glacier GPS stations. Locations of the stations shown in figure 12. Raw position data were filtered to remove spurious spikes and interpolated to 0.2-d intervals. Estimated error is 0.05 m/d. ICY4 and ICY5 were on glacier in mid- to late winter 2005 while the new lava dome was expanding eastward. ELE4 was fortuitously placed on glacier about the time that dome growth to east stopped, and it stayed on the glacier until early summer 2005. HIE5 was on the glacier in mid-summer 2005. Azimuth of motion for all stations was within 18° of north. Shown for comparison are surface-speed data (adapted from Anderson and others, 2005) for a target on Kennicott Glacier, a temperate valley glacier in Alaska, during the year 2000. The record for Kennicott Glacier shows large-amplitude, commonly diurnal fluctuations not seen at east Crater Glacier.

period were analyzed to determine direction and magnitude of the principal strain rates within the (approximately horizontal) plane determined by the three stations. Unsurprisingly, the direction of principal compression lined up closely with the trend of crevasses that formed during westward dome growth (fig. 17). Magnitudes of principal horizontal strain rates increased slowly over time, with their sum consistently negative at about –0.002/d. Making the plausible interpretation that surface uplift represents thickening of the glacier, vertical strain rate can be estimated as the average uplift rate divided by the glacier thickness, or about (0.25 m/d)/(120 m) = 0.002/d. The sum of the three principal strain rates was thus locally near zero, consistent with bulk incompressibility.

In 2006, we had motion data for three GPS stations located on WCG downglacier of the region being squeezed by the lava dome: DAVF, which operated for several months (during which time the station was relocated three times to prevent it from toppling into a crevasse), and JOEA and JOEC, which operated for about six weeks during summer (fig. 24). Station DAVF was slightly upglacier of the cross section H–I (fig. 13*A*), on ice that thickened steadily as west Crater Glacier was squeezed (fig. 19*D*). Although the motion record for DAVF (fig. 24*A*) is complicated by the effect of crevasse growth and the need to move the instrument, there is again an absence of the diurnal speed variation we would expect if glacier sliding were occurring. The motion records for JOEA and JOEC (fig. 24*B*), located only about 150 m apart, nicely document deformation associated with the shear zone shown in figure 20. Station JOEA (east of the shear zone), on ice being shoved as the bulge in the WCG surface propagates downglacier and impinges upon the terminus region, moved nearly three times as fast as JOEC (west of the shear zone). The difference in azimuth of motion between JOEA and JOEC almost certainly reflects the opening of roughly north-south-striking crevasses (fig. 20).

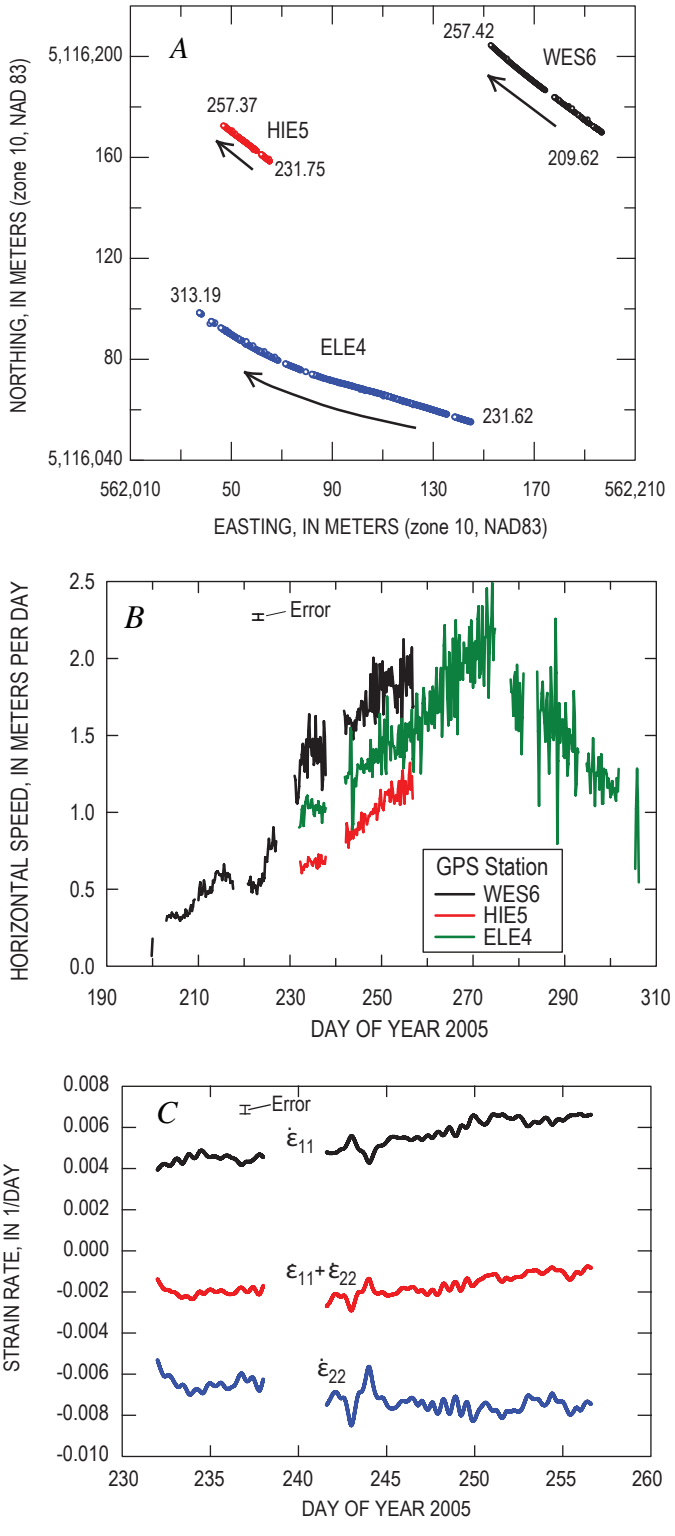

Inferences About Glacier and Volcano Hydrology

Temperate glaciers (those with ice at the melting point) move by a combination of internal creep and sliding of the ice over the bed (van der Veen, 1999). The creep component reflects the internal stress state of the glacier rather than conditions at the bed, whereas the sliding component reflects the boundary condition at the bed—in particular, how much friction there is against the bed. Measurements at many

Figure 23. GPS-derived motion data for west Crater Glacier in 2005. *A*, Displacement trajectories projected into horizontal plane, with day of year at beginning and end indicated. *B*, Horizontal speeds, calculated by filtering raw position data to remove spurious spikes, interpolating to 0.2-d intervals, and applying centered difference. Estimated error, shown by error bar, is 0.05 m/d. As with the east Crater Glacier record (fig. 22), diurnal speed fluctuations are not seen at west Crater Glacier. *C*, Principal strain rates in horizontal plane. Orientation of maximum extension ($\dot{\varepsilon}_{11}$) is N. 10° E.–S. 10° W.; orientation of maximum compression ($\dot{\varepsilon}_{22}$) is N. 80° W.–S. 80° E. For strictly incompressible ice, the sum $\dot{\varepsilon}_{11}+\dot{\varepsilon}_{22}$ would be zero.

glaciers have shown systematic differences between surface speed during the ablation (melt) season and during winter. For example, pulses of increased surface speed are commonly observed as the melt season begins (Anderson and others, 2004). More generally, surface speed in summer is higher than in winter, and large diurnal variations in surface speed are common (Fountain and Walder, 1998). As the creep component of glacier motion should be reasonably constant, variations in surface speed reflect variations in sliding speed, which is modulated by meltwater at the bed (see, for example, Harper and others, 2002). Our 2005 data for east Crater Glacier (fig. 22), however, show neither acceleration with the onset of the melt season nor a clear diurnal signal; data for west Crater Glacier from the summers of 2005 and 2006 (figs. 23, 24) similarly lack any diurnal signal. We propose as an explanation that there simply is no pressurized drainage system conveying water along the bed. Crater Glacier grew atop several tens of meters of rubble (mainly rock-avalanche debris) that had accumulated on the crater floor following the eruption of May 18, 1980 (Mills, 1992). As argued in appendix 1, much of this rubble is likely to be ice free because geothermal heat flow will have melted interstitial ice, and flow of the overlying ice downward into the rubble will have been slow. The volcanic edifice beneath this rubble is geologically complex, consisting of multiple lava flows, pyroclastic and lahar deposits, and other fragmental deposits (Crandell, 1987). Thus, water that reaches the glacier bed probably flows out of the crater through the rubble layer or downward into the volcano's groundwater system, rather than moving along the glacier bed. In support of this hypothesis, we note that there are no outlet streams at the glacier termini, although there are springs and seeps farther downslope. Discharge in Loowit Creek, which heads several hundred meters downstream of the WCG and ECG termini and drains the crater, is not measured regularly, owing to the impossibility of maintaining a permanent gaging station in the very unstable stream channel. However, such occasional discharge measurements as have been made (fig. 25) show no evidence for systematically elevated streamflow during the eruption.

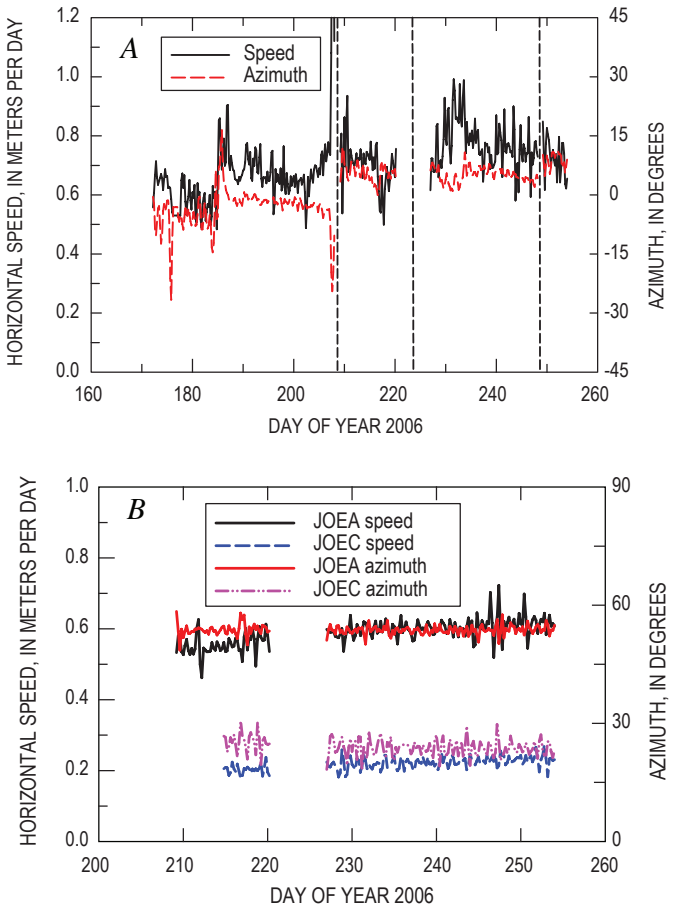

Figure 24. Motion data for GPS stations on the surface of west Crater Glacier in 2006. Estimated errors about 0.05 m/d for speed and 2 degrees for azimuth. See figure 13*B* for locations of the GPS stations. *A*, Horizontal speed and azimuth of GPS station DAVF. Dashed lines indicate breaks in data when instrument was moved to keep it from toppling into crevasses that formed during its stay. *B*, Horizontal speed and azimuth of GPS stations JOEA and JOEC.

Inferences from Glacier Dynamics Bearing on Lava-Dome Mechanics

We envisage outward push on Crater Glacier by the expanding Mount St. Helens dome as involving not glacier sliding, as usually considered by glaciologists, but low-angle thrust faulting. In our view, the glacier is being pushed over the underlying unconsolidated rock debris, with the décollement probably near the glacier bed (glacier bed being a rather ill-defined concept in the present case, as discussed earlier). Our conception of the process is sketched in figure 26. Glacier deformation

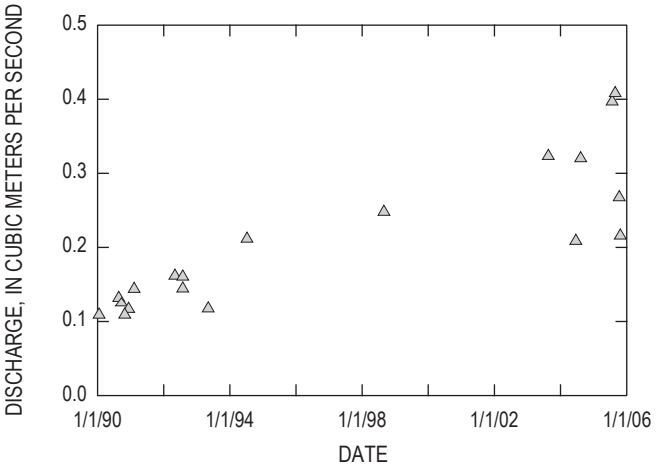

Figure 25. Discharge in Loowit Creek measured above Loowit Falls, from unpublished streamflow data collected by hydrologic surveillance staff at Cascades Volcano Observatory. Probable error in measurements is about 10 percent.

is for all intents and purposes quasistatic—accelerations can be ignored—so conservation of momentum reduces to a force balance. The force exerted by the lava dome will be balanced by the sum of resisting forces within the ice and at the glacier bed,

$$p \approx \left|\tau_{nn}\right| + (W/H)\tau_b, \qquad (2)$$

where p is the pressure (force per unit area) exerted by the lava dome, τ_{nn} is the deviatoric stress within the ice normal to the dome-glacier contact, W is the width of the glacier (that is, the distance from the dome to the crater wall), H is a typical value of ice thickness, and τ_b is the magnitude of the shear stress opposing displacement of the glacier in a direction normal to the dome-ice margin (fig. 26). If motion on the décollement involves essentially Coulomb friction (that is, frictional resistance proportional to the normal load), then $\tau_b \approx \mu\rho_i gH$, where μ is the coefficient of friction, ρ_i is the density of ice, and g is acceleration due to gravity, and our estimate for p becomes

$$p \approx \left|\tau_{nn}\right| + \mu\rho_i gW. \qquad (3)$$

We have taken the normal stress on the décollement to be equal to the ice-overburden pressure. Thus we are supposing that water pressure on the décollement is negligible, as is reasonable, because, as noted above, water at the glacier bed apparently flows downward into the volcano rather than in a pressurized drainage system along the bed.

We now estimate the magnitude of the two terms on the right-hand side of equation 3. The deviatoric stress within the ice normal to the dome-glacier contact, τ_{nn}, can be estimated if we take into account the rheological behavior of glacier ice as (see appendix 3):

$$\tau_{nn} = B\left|\dot{\varepsilon}_e\right|^{-2/3}\dot{\varepsilon}_{nn}, \qquad (4)$$

where $\dot{\varepsilon}_{nn}$ is the strain rate normal to the dome-glacier contact and the so-called effective strain rate $\dot{\varepsilon}_e$ (equal to one-half the second invariant of the strain-rate tensor) is in this case given by

$$2\dot{\varepsilon}_e^{\,2} = \dot{\varepsilon}_{nn}^2 + \dot{\varepsilon}_{tt}^2 + \dot{\varepsilon}_{zz}^2, \qquad (5)$$

where $\dot{\varepsilon}_{tt}$ is the strain rate tangential to the dome-glacier contact and $\dot{\varepsilon}_{zz}$ is the vertical strain rate. In writing equation 5, we assume that the directions normal and tangential to the dome-glacier contact are the directions of principal strain rates, an assumption that is supported by the available data. Using $B = 5.3\times10^7$ Pa·s$^{1/3}$ (Paterson, 1994; van der Veen, 1999) and the strain-rate calculations given above, we estimate $\left|\tau_{nn}\right| \approx$ 0.16–0.21 MPa. Taking $\mu \approx 0.5$ (consistent with there being considerable debris within the ice and thus much rock-to-rock friction at the décollement), $\rho_i = 900\,\mathrm{kg/m^3}$ (corresponding to glacier ice, not snow or firn), $g = 9.8$ m/s^2, and $W \approx 250$ m, the frictional term on the right-hand side of equation 3 has a magnitude of about 1.1 MPa. Frictional resistance on the décollement therefore dominates the force balance, with the estimated value of p being about 1.3 MPa. This estimate is admittedly rough, as we have not factored in the complicated geometry of the real system.

Summary and Outlook for the Future

The eruption of Mount St. Helens that began in fall 2004 has presented us with the first-ever opportunity to observe and document emplacement of a lava dome through glacier ice. The eruption has not caused any rapid melting of Crater Glacier, but the effects on the glacier have nonetheless been striking. Dome growth cut the glacier in two and then successively squeezed the two parts. Measurements using both specialized, helicopter-deployed GPS stations and photogrammetrically derived DEMs showed that the two glaciers underwent deformation of an extreme variety, with strain rates of extraordinary magnitude as compared to those in normal alpine temperate glaciers. Moreover, the GPS-derived motion records make clear that Crater Glacier is fundamentally unlike normal alpine glaciers, in that there is no evidence that it slides over its bed. The most reasonable explanation for this anomaly is that meltwater reaching the glacier bed enters the volcano's groundwater system rather than flowing toward the glacier terminus through a drainage network along the bed.

The part of east Crater Glacier that underwent thickening has been thinning since dome growth shifted to the west in April 2005, and normal ice flow has moved mass downstream. Terminus advance is likely to continue unless eruptive processes remove substantial glacier mass. West Crater Glacier is likely to evolve similarly in the short term, with terminus dynamics complicated by the formation of the shear zone shown in figure 20. The pattern of snow accumulation in the crater has been radically perturbed, with heat from the new lava dome locally preventing accumulation. Sufficiently prolonged dome growth could, of course, completely eliminate ice from the crater (and indeed completely eliminate the crater itself). Glaciers at Mount St. Helens come and go, modulated by the style and rhythm of eruptive behavior.

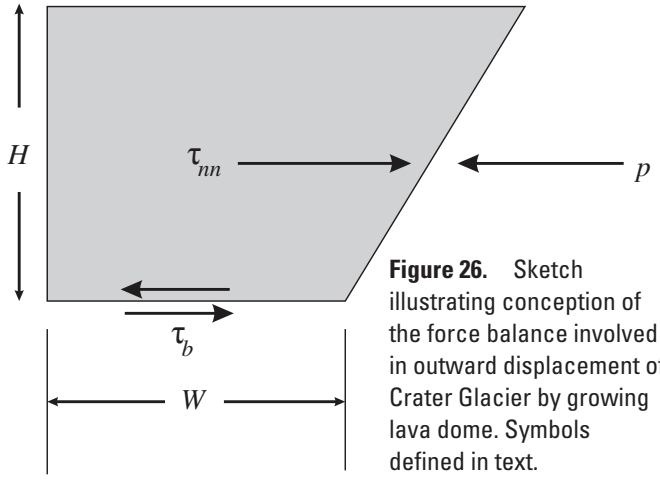

Figure 26. Sketch illustrating conception of the force balance involved in outward displacement of Crater Glacier by growing lava dome. Symbols defined in text.

Acknowledgments

R.M. Iverson and S.P. Anderson made helpful comments on an earlier version of this manuscript. DEMs were prepared by J. Messerich of the U.S. Geological Survey Photogrammetric Lab, Denver, Colorado, using aerial photographs taken by Bergman Photographic Services.

References Cited

Anderson, R.S., Anderson, S.P., MacGregor, K.R., Waddington, E.D., O'Neel, S., Riihimaki, C.A., and Loso, M.G., 2004, Strong feedbacks between hydrology and sliding of a small alpine glacier: Journal of Geophysical Research (Earth Surfaces), v. 109, F03005, 17 p., doi:10.1029/2004JF000120.

Anderson, R.S., Walder, J.S., Anderson, S.P., Trabant, D.C., and Fountain, A.G., 2005, The dynamic response of Kennicott Glacier to the Hidden Creek Lake outburst flood: Annals of Glaciology, v. 40, p. 237–242.

Brugman, M.M., and Meier, M.F., 1981, Response of glaciers to the eruptions of Mount St. Helens, *in* Lipman, P.W., and Mullineaux, D.R., eds., The 1980 eruptions of Mount St. Helens, Washington: U.S. Geological Survey Professional Paper 1250, p. 743–756.

Crandell, D.R., 1987, Deposits of pre-1980 pyroclastic flows and lahars from Mount St. Helens volcano, Washington: U.S. Geological Survey Professional Paper 1444, 91 p.

Fountain, A.G., and Walder, J.S., 1998, Water flow through temperate glaciers: Reviews of Geophysics, v. 36, no. 3, p. 299–328.

Gilbert, J.S., Stasiuk, M.V., Lane, S.J., Adam, C.R., Murphy, M.D., Sparks, R.S.J., and Naranjo, J.A., 1996, Non-explosive, constructional evolution of the ice-filled caldera at Volcán Sollipulli, Chile: Bulletin of Volcanology, v. 58, no. 1, p. 67–83.

Guðmundsson, M.T., Sigmundsson, F., and Björnsson, H., 1997, Ice–volcano interaction of the 1996 Gjálp subglacial eruption, Vatnajökull, Iceland: Nature, v. 389, no. 6654, p. 954–957.

Hallet, B., 1979, A theoretical model of glacial abrasion: Journal of Glaciology, v. 23, no. 89, p. 321–334.

Harper, J.T., Humphrey, N.F., and Greenwood, M.C., 2002, Basal conditions and glacier motion during the winter/spring transition, Worthington Glacier, Alaska, U.S.A.: Journal of Glaciology, v. 48, no. 160, p. 42–50.

Iverson, N.R., and Semmens, D., 1995. Intrusion of ice into porous media by regelation; a mechanism of sediment entrainment by glaciers: Journal of Geophysical Research, v. 100, no. B6, p. 10219–10230.

Kamb, B., Raymond, C.F., Harrison, W.D., Engelhardt, H., Echelmeyer, K.A., Humphrey, N., Brugman, M.M., and Pfeffer, T., 1985, Glacier surge mechanism; 1982–1983 surge of Variegated Glacier, Alaska: Science, v. 227, no. 4686, p. 469–479.

LaHusen, R.G., Swinford, K.J., Logan, M., and Lisowski, M., 2008, Instrumentation in remote and dangerous settings; examples using data from GPS "spider" deployments during the 2004–2005 eruption of Mount St. Helens, Washington, chap. 16 *of* Sherrod, D.R., Scott, W.E., and Stauffer, P.H., eds., A volcano rekindled; the renewed eruption of Mount St. Helens, 2004–2006: U.S. Geological Survey Professional Paper 1750 (this volume).

Major, J.J., and Newhall, C.G., 1989, Snow and ice perturbations during historical volcanic eruptions and the formation of lahars and floods: Bulletin of Volcanology, v. 52, no. 1, p. 1–27.

Mills, H.H., 1992, Post-eruption erosion and deposition in the 1980 crater of Mount St. Helens, Washington, determined from digital maps: Earth Surface Processes and Landforms, v.17, no. 8, p. 739–754.

Murav'ev, Ya.D., and Salamatin, A.N., 1990, Mass balance and thermal regime of a crater glacier at Ushkovskii Volcano: Volcanology and Seismology, v. 11, no. 3, p. 411–424.

Paterson, W.S.B., 1994, The physics of glaciers (3d ed.): Oxford, Pergamon, 480 p.

Philip, J.R., 1980, Thermal fields during regelation: Cold Regions Science and Technology, v. 3, nos. 2–3, p. 193–203.

Price, S.F., and Walder, J.S., 2007, Modeling the dynamic response of a crater glacier to lava-dome emplacement: Mount St. Helens, Washington, U.S.A.: Annals of Glaciology, v. 45, no. 1, p. 21–28, doi:10.3189/172756407782282525.

Raymond, C.F., 1987, How do glaciers surge?: Journal of Geophysical Research, v. 92, no. B9, p. 9121–9134.

Raymond, C., Johannesson, T., Pfeffer, T., and Sharp. M., 1987, Propagation of a glacier surge into stagnant ice: Journal of Geophysical Research, v. 92, no. B9, p. 9037–9049.

Salamatin, A.N., and Murav'ev, Ya.D., 1992, Some results of a study of the physical characteristics of the glacial stratum on the slopes of the Klyuchevskoy volcano: Volcanology and Seismology, v. 13, no. 2, p. 230–240.

Schilling, S.P., Carrara, P.E., Thompson, R.A., and Iwatsubo, E.Y., 2004, Posteruption glacier development within the crater of Mount St. Helens, Washington, USA: Quaternary

Research, v. 61, no. 3, p. 325–329.

Schilling, S.P., Thompson, R.A., Messerich, J.A., and Iwatsubo, E.Y., 2008, Use of digital aerophotogrammetry to determine rates of lava dome growth, Mount St. Helens, Washington, 2004–2005, chap. 8 *of* Sherrod, D.R., Scott, W.E., and Stauffer, P.H., eds., A volcano rekindled; the renewed eruption of Mount St. Helens, 2004–2006: U.S. Geological Survey Professional Paper 1750 (this volume).

Schneider, D.J., Vallance, J.W., Wessels, R.L., Logan, M., and Ramsey, M.S., 2008, Use of thermal infrared imaging for monitoring renewed dome growth at Mount St. Helens, 2004, chap. 17 *of* Sherrod, D.R., Scott, W.E., and Stauffer, P.H., eds., A volcano rekindled; the renewed eruption of Mount St. Helens, 2004–2006: U.S. Geological Survey Professional Paper 1750 (this volume).

Simons, F.S., and Mathewson, D.E., 1955, Geology of Great Sitkin Island, Alaska: U.S. Geological Survey Bulletin 1028–B, 43 p.

Tuffen, H., Gilbert, J., and McGarvie, D., 2001, Products of an effusive subglacial rhyolite eruption; Bláhnúkur, Torfajökull, Iceland: Bulletin of Volcanology, v. 63, nos. 2–3, p. 179–190.

Vallance, J.W., Schneider, D.J., and Schilling, S.P., 2008, Growth of the 2004–2006 lava-dome complex at Mount St. Helens, Washington, chap. 9 *of* Sherrod, D.R., Scott, W.E., and Stauffer, P.H., eds., A volcano rekindled; the renewed eruption of Mount St. Helens, 2004–2006: U.S. Geological Survey Professional Paper 1750 (this volume).

van der Veen, C.J., 1999, Fundamentals of glacier dynamics: Rotterdam, A.A. Balkema, 462 p.

Walder, J.S., LaHusen, R.G., Vallance, J.W., and Schilling, S.P., 2005, Crater glaciers on active volcanoes; hydrological anomalies: Eos (American Geophysical Union Transactions), v. 86, no. 50, p. 521, 528.

Walder, J.S., LaHusen, R.G., Vallance, J.W., and Schilling, S.P., 2007, Emplacement of a silicic lava dome through a crater glacier; Mount St Helens, 2004–06: Annals of Glaciology, v. 45, no. 1, p. 14–20, doi:10.3189/172756407782282426.

Appendix 1. Interstitial Ice in Crater-Floor Rock Debris

As shown by Mills (1992) and noted above, until about 1986, material accumulating on the Mount St. Helens crater floor consisted primarily of rock-avalanche material with interstitial snow. After 1986, the volumetric rate of snow accumulation exceeded the accumulation rate of rock debris. By the time the 2004 eruption began, the crater-fill material was locally as thick as 200 m, and it is hard to envisage that any interstitial snow within the lowermost fill would not have transformed to glacier ice (Paterson, 1994). However, there is reason to believe that some of the deepest fill may in fact be ice free, because interstitial ice within the rock framework will be melted by geothermal heat and not replaced by ice from above. If all heat flux from below causes melting, then the melt rate $\dot{m}$, expressed as thickness per unit time, will be given by the ratio of the geothermal heat flux, q_G, to the energy required to melt a unit volume of ice,

$$\dot{m} = \frac{q_G}{\phi \rho_i L}, \qquad (6)$$

where ϕ is porosity of the avalanche debris, ρ_i is the density of ice, and L is the heat of fusion. If one considers a glacier in a nonvolcanic setting, then taking $\phi = 0$, $L = 3.35 \times 10^5$ J/kg, and $q_G = 0.05$ W/m^2, one finds $\dot{m} \approx 5$ mm/yr. In a volcanic setting, q_G could easily be one hundred times greater (Murav'ev and Salamatin, 1990; Salamatin and Murav'ev, 1992), and taking $\phi \approx 0.4$ for the crater-fill avalanche debris, one finds $\dot{m} \approx 1$ m/yr. Clearly melting can proceed rapidly, although we stress that these estimates for $\dot{m}$ are upper bounds, because ground water could carry away some of the geothermal heat flux.

The rate at which overlying glacier ice can flow into the avalanche debris is very low. The ice intrusion rate V is proportional to the gradient of ice pressure across the debris layer (Iverson and Semmens, 1995):

$$V = K_s P_g, \qquad (7)$$

where P_g is the gradient of ice pressure across the debris layer, and the proportionality constant K_s is analogous to hydraulic conductivity for ground-water flow. The constant K_s can be determined on theoretical grounds (Philip, 1980) in the case that the debris grain size is small enough that ice flow is dominantly by regelation, with plastic creep negligible; experimental results of Iverson and Semmens (1995) support Philip's theory. The crater-fill debris is coarse enough that plastic creep is necessary for the ice to flow through the pore space (Hallet, 1979), so the regelation-only value $K_S \approx 3 \times 10^{-15}$ m^2/Pa·s will give an overestimate of V. The ice pressure gradient P_g obviously depends upon the thickness of the ice-filled debris layer and the pressure of the overlying ice. For present purposes, suppose that the overburden pressure is 1 MPa (corresponding to an ice thickness of about 110 m) and the thickness of the ice-filled debris layer is 10 m. We then find from equation 7 that an upper-bound estimate of V is about 0.01 m/yr. A balance between $\dot{m}$ and V can exist only if the ice-filled debris layer is very thin—a few centimeters at most. We conclude that the ice within the deepest crater fill ought to, over time, melt out and not be replenished. It seems likely that the deepest crater fill will act as an aquifer conveying water along the crater floor toward the glacier terminus.

Appendix 2. Calculating Glacier Volume

The change in total glacier volume within the crater of Mount St. Helens, over the course of the eruption, was determined by GIS methods. Details of the method can be understood with reference to figure 27. The area covered by the glacier before the eruption was broken into three parts: part A1 includes the area within which dome rock was emplaced, and parts A2 and A3 are the east and west glacier arms that were not disrupted directly by dome growth. The glacier volumes in A2 and A3 were determined by differencing DEMs for various dates with the October–November 1986 DEM, the latter representing, as we argued in the main text, approximately the bed of the crater glacier.

As we are only trying to track the change in glacier volume with time, rather than total glacier volume, the exact choice of datum for the bed is not critical. (The ambiguity in determining the bed, upon which we commented in the main text, is thus not a problem.) The glacier volume in A1 is calculated as follows: Using the 1986 DEM as the datum, let the difference between the total volume above this surface at some date τ be denoted by V_τ, and the volume of extruded dome rock within A1 be given by V_d. (The calculation of V_d. is described by Schilling and others, this volume, chap. 8.) The glacier volume within A1 is then $V_\tau - V_d$. This volume is added to the volumes in A2 and A3 to get the total glacier volume. The error in this total volume can be estimated as the total glacier surface area (1.0 km^2) times the root-mean-square error in the elevation-differencing procedure, which we take as 2.5 m. (This value follows from the 2.5 m error on the 1986 DEM, which was produced from a topographic map with contour interval of 5 m, and the 0.1 to 0.2 m error on later DEMs, which were produced directly from aerial photographs.

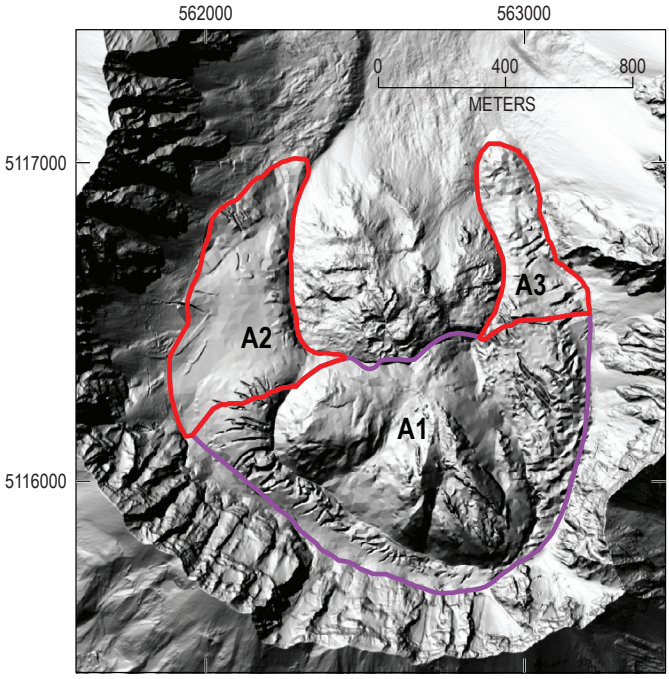

Figure 27. Separation of crater DEM coverages into three sections used in calculating total glacier volume as given in figure 21. Area A1 overlaps new lava dome, whereas areas A2 and A3 correspond to the downstream arms of west Crater Glacier and east Crater Glacier, respectively. Method of volume calculation is described in appendix 2. Background is hillshade-relief map based on DEM of October 24, 2005. Coodinates are UTM zone 10 easting and northing, North America datum 1983.

Appendix 3. Glacier Flow Dynamics

The flow law of ice is an empirical relation between stress and strain rate. For isotropic ice, the flow law is customarily written as the tensor relation (van der Veen, 1999)

$$\tau_{ij} = 2\eta\dot{\varepsilon}_{ij}\,, \tag{8}$$

where τ_{ij} are deviatoric stresses, $\dot{\varepsilon}_{ij}$ are strain rates, and η is an effective viscosity that depends on the overall strain-rate field:

$$\eta = (B/2)\,\dot{\varepsilon}_e^{\,(1/n)-1}\,. \tag{9}$$

B is a material property that depends on temperature, $n \approx 3$ for glacier ice (as compared to $n = 1$ for a Newtonian-viscous fluid like water), and $\dot{\varepsilon}_e$ is the effective strain rate, defined by the relation

$$2\dot{\varepsilon}_e^{\,2} = \dot{\varepsilon}_{xx}^2 + \dot{\varepsilon}_{yy}^2 + \dot{\varepsilon}_{zz}^2 + 2(\dot{\varepsilon}_{xy}^2 + \dot{\varepsilon}_{xz}^2 + \dot{\varepsilon}_{yz}^2)\,. \tag{10}$$

Here x, y, and z are arbitrary orthogonal coordinates. In the simple case of unidirectional slab flow—that is, flow driven by gravity and resisted by drag on the base (see, for example, van der Veen, 1999)—one could choose x as the downglacier coordinate, y as the cross-glacier coordinate, and z as normal to the glacier surface. The only nonzero strain-rate component would then be $\dot{\varepsilon}_{xz}$, in which case $\dot{\varepsilon}_e = |\dot{\varepsilon}_{xz}|$ and the flow law becomes a simple relation between shear stress and shear strain rate,

$$\tau_{xz} = B\,|\dot{\varepsilon}_{xz}|^{(1/n)-1}\dot{\varepsilon}_{xz}\,. \tag{11}$$

We argued in the main text above that the crater glacier probably does not slide over its bed. The average strain rate $\dot{\varepsilon}_{xz}$ may therefore be estimated simply as the surface speed U divided by the glacier thickness H. Taking $U \approx 1$ m/d and $H \approx 150$ m in the part of east Crater Glacier experiencing lateral squeeze (see, for example, station ICY5 on fig. 14), the magnitude of the average strain rate $\dot{\varepsilon}_{xz}$ is then about 6.7×10^{-3}/d, comparable to the magnitude of the lateral strain rate $\dot{\varepsilon}_{yy}$ and vertical strain rate $\dot{\varepsilon}_{zz}$, which, as noted in the main text, averaged about 3×10^{-3}/d over the period of squeezing. The value $\dot{\varepsilon}_e$ is not well approximated by $|\dot{\varepsilon}_{xz}|$ in this case, and the nonzero (and in fact relatively large) values of $\dot{\varepsilon}_{yy}$ and $\dot{\varepsilon}_{zz}$ substantially reduce the effective viscosity (see equations 9 and 10).

In the slab-flow model, shear stress is simply proportional to depth and surface slope; that is, $\tau_{xz} = \rho_i g z \sin\theta$, where θ is surface slope and z increases downward from the glacier surface. One then finds that U depends upon flow ice thickness and slope according to the expression

$$U = \frac{2H}{n+1}\left(\frac{\rho_i g H \sin\theta}{B}\right)^n. \tag{12}$$

With the usual value $n = 3$, the surface speed then varies as H^4.